

Electronic Supporting Information

Mesoporous Carbon Capsules as Electrode Materials in Electrochemical Double Layer Capacitors

Shanthi Murali,^{a,§} Daniel R. Dreyer,^{b,§} Patricia Valle-Vigón,^c Meryl D. Stoller,^a Yanwu Zhu,^a Cornelio Morales,^a Antonio B. Fuertes,^c Christopher W. Bielawski,^{b,} Rodney S. Ruoff^{a,*}*

^a Department of Mechanical Engineering and the Texas Materials Institute, The University of Texas at Austin, 1 University Station C2200, Austin, Texas, 78712 USA

^b Department of Chemistry and Biochemistry, The University of Texas at Austin, 1 University Station A5300, Austin, Texas, 78712 USA

^c Instituto Nacional del Carbon (CSIC), P.O. Box 73, 33080, Oviedo, Spain

*E-mail: bielawski@cm.utexas.edu; r.ruoff@mail.utexas.edu

Synthetic Details	S2–S6
General Considerations	S2
Synthetic Procedures	S2–S6
Characterization of Mesoporous Carbon Capsules	S7–S8
Figure S1. SEM image of carbon capsules.	S7
Figure S2. PXRD pattern of carbon capsules.	S8
EDLC Performance Analyses	S9–S20
Figure S3. Schematic of two-electrode test cell assembly.	S9
Figure S4. EDLC performance of the carbon capsules in aq. KOH.	S11
Figure S5. EDLC performance of the carbon capsules in 1 M TEA BF ₄ in AN.	S12
Figure S6. EDLC performance of the carbon capsules in IL 3 (BMIM PF ₆).	S13
Figure S7. EDLC performance of the carbon capsules in IL 4 .	S14
Figure S8. EDLC performance of the carbon capsules in IL 5 .	S15
Figure S9. EDLC performance of the carbon capsules in IL 7 .	S16
Figure S10. EDLC performance of the carbon capsules in IL 8 .	S17
Figure S11. EDLC performance of the carbon capsules in IL 9 .	S18
Figure S12. EDLC performance of MEGO in IL 6 .	S19
Figure S13. EDLC performance of CReGO in IL 6 .	S20
References	S21

[§] S. Murali and D. R. Dreyer contributed equally to this work.

General Considerations. Unless otherwise noted, all reactions were performed under ambient conditions. All reagents were purchased from Acros Organics, TCI America, Sigma Aldrich, or Alfa Aesar and were distilled prior to use. ^1H and ^{13}C NMR data were collected on Varian Unity INOVA 400 MHz or Varian Mercury 300 MHz spectrometers. Chemical shifts (δ) are referenced downfield from $(\text{CH}_3)_4\text{Si}$ using the residual solvent peak as an internal standard (CDCl_3 , 7.24 ppm for ^1H and 77.0 ppm for ^{13}C NMR, respectively). ^{19}F NMR spectra were acquired on a Varian 400 MHz DirectDrive spectrometer and referenced to an external standard (^{19}F : CFCl_3 , 0 ppm). High-resolution mass spectra (HRMS) were obtained with a VG analytical ZAB2-E instrument (ESI or CI). Unless otherwise noted, all glass transition temperatures (T_g) and/or melting points (T_m) were measured using a Mettler Toledo DSC 823e. Decomposition temperatures (T_d) were obtained using a Mettler Toledo TGA/SDTA 851. Elemental analyses were performed by Midwest Microlabs, LLC (Indianapolis, IN). Scanning electron microscopy (SEM) images were collected on a FEI Quanta-600 FEG Environmental SEM. Powder X-ray diffraction (PXRD) analysis were collected on a Phillips X'Pert PRO ($\lambda = 1.5405 \text{ \AA}$). Determination of specific surface areas was carried out on a Quantachrome Instruments Nova 2000 using nitrogen as the adsorbent.

N-methyl-N-(n-octyl)piperidinium bromide. Using a modified literature procedure,¹ a 50 mL round bottom flask was charged with N-methylpiperidine (4.4350 g; 4.47×10^{-2} mol) and acetonitrile (35 mL). To the resulting solution was added 1-bromooctane (8.7136 g; 4.51×10^{-2} mol). After heating the reaction mixture at 50 °C for 14 h, the solvent was removed under reduced pressure and the residual solid was triturated and sonicated in diethyl ether (3×40 mL), which was then decanted off. Subsequent drying under vacuum afforded the desired product as an off-white, hygroscopic powder (13.0658 g, 97% yield). m.p. 183–185 °C (determined using a Mel-Temp apparatus). ^1H NMR (300 MHz, CDCl_3): 3.77 (m, 2H), 3.62 (m, 4H), 3.31 (s, 3H), 1.90-1.66 (m, 8H), 1.27-1.18 (m, 10H), 0.83 (t, $J = 7$ Hz, 3H). ^{13}C NMR (75 MHz, CDCl_3): 62.7, 60.4, 47.7, 31.2, 28.7, 28.6, 25.9, 22.1, 21.6, 20.2, 19.8, 13.6. $T_d = 216.42$ °C. HRMS Calcd. for $\text{C}_{14}\text{H}_{30}\text{N} [\text{M}^+]$: 212.2376. Found: 212.2379. Anal. Calcd for $\text{C}_{14}\text{H}_{30}\text{NBr}$: C, 57.53; H, 10.34; N, 4.79. Found: C, 57.48; H, 10.36; N, 4.79.

N-methyl-N-(n-octyl)piperidinium bis(trifluoromethanesulfonyl)imide (4). Using a modified literature procedure,¹ a 40 mL vial was charged with N-methyl-N-(n-octyl)piperidinium bromide

(1.1547 g; 3.95×10^{-3} mol) and deionized water (35 mL). The resulting suspension was then charged with lithium bis(trifluoromethanesulfonyl)imide (1.1690 g; 4.07×10^{-3} mol), and the vial was sealed with a Teflon-lined cap. The resulting solution was then stirred vigorously at room temperature for 14 h, after which time a yellow liquid was observed to phase separate at the bottom of the vial. The supernatant was decanted and the residual yellow liquid was triturated and sonicated in water (3×35 mL) to remove unreacted starting materials. Subsequent drying under vacuum afforded the desired product as a viscous yellow liquid (1.8679 g, 96% yield). ^1H NMR (400 MHz, CDCl_3): 3.30 (t, $J = 7$ Hz, 4H), 3.22 (t, $J = 7$ Hz, 2H), 2.96 (s, 3H), 1.87 (br, 4H), 1.64 (br, 4H), 1.38 (m, 4H), 1.21 (m, 6H), 0.82 (t, $J = 7$ Hz, 3H). ^{13}C NMR (100 MHz, CDCl_3): 119.8 (q, $J = 320$ Hz), 64.3, 61.2, 47.5, 31.5, 28.8, 28.8, 26.0, 22.4, 21.6, 20.5, 19.8, 13.9. ^{19}F NMR (376 MHz, CDCl_3): -79.0 . $T_g = -72.68$ °C. $T_d = 415.62$ °C. HRMS Calcd. for $\text{C}_{14}\text{H}_{30}\text{N} [\text{M}^+]$: 212.2376. Found: 212.2371. Anal. Calcd for $\text{C}_{16}\text{H}_{30}\text{F}_6\text{N}_2\text{O}_4\text{S}_2$: C, 39.02; H, 6.14; N, 5.69. Found: C, 39.16; H, 6.11; N, 5.53.

N-methyl-N-(n-octyl)piperidinium trifluoromethanesulfonate (5). Using a modified literature procedure,² a 40 mL vial was charged with N-methyl-N-(n-octyl)piperidinium bromide (1.0393 g; 3.56×10^{-3} mol) and dichloromethane (35 mL) under nitrogen. This solution was charged with methyl trifluoromethanesulfonate (0.5 mL; 4.4×10^{-3} mol) slowly via syringe at room temperature; an exotherm and gas evolution were observed. The reaction vessel was then sealed with a septum, stirred at room temperature for 6 h, after which time the solvent was removed under reduced pressure. The residual solid was triturated and sonicated in diethyl ether (3×35 mL) to remove unreacted starting materials. Subsequent drying under vacuum afforded the desired product as an off-white solid (1.2724 g, 99% yield). ^1H NMR (400 MHz, CDCl_3): 3.39 (m, 4H), 3.30 (t, $J = 7$ Hz, 2H), 3.04 (s, 3H), 1.87 (m, 4H), 1.63 (m, 4H), 1.35 (m, 4H), 1.22 (m, 6H), 0.84 (t, $J = 7$ Hz, 3H). ^{13}C NMR (100 MHz, CDCl_3): 120.4 (q, $J = 320$ Hz), 63.6, 60.9, 47.9, 31.5, 28.9, 28.9, 26.1, 22.4, 21.7, 20.6, 19.9, 13.9. ^{19}F NMR (376 MHz, CDCl_3): -78.6 . $T_m = 42.39$ °C. $T_d = 363.22$ °C. HRMS Calcd. for $\text{C}_{14}\text{H}_{30}\text{N} [\text{M}^+]$: 212.2376. Found: 212.2371. Anal. Calcd for $\text{C}_{15}\text{H}_{30}\text{F}_3\text{NO}_3\text{S}$: C, 49.84; H, 8.37; N, 3.87. Found: C, 49.71; H, 8.33; N, 3.94.

N-methyl-N-(n-octyl)pyrrolidinium bromide. Using a modified literature procedure,³ a 40 mL vial was charged with N-methylpyrrolidine (5.1024 g; 5.99×10^{-2} mol) and acetonitrile (35 mL). The resulting solution was then charged with 1-bromooctane (11.7079 g; 6.06×10^{-2} mol) and

the vial was sealed with a Teflon-lined cap. After heating the reaction mixture at 100 °C for 12 h, the solvent was removed under reduced pressure and the residual solid was triturated and sonicated in diethyl ether (3×100 mL) to remove unreacted starting materials. Subsequent drying under vacuum afforded the desired product as a white, hygroscopic powder (16.0016 g, 95 % yield). m.p. = 148–151 °C (determined using a Mel-Temp apparatus). ^1H NMR (400 MHz, CDCl_3): 3.70 (t, $J = 7$ Hz, 4H), 3.50 (t, $J = 7$ Hz, 2H), 3.15 (s, 3H), 2.16 (t, $J = 7$ Hz, 4H), 1.61 (br, 2H), 1.23 (m, 4H), 1.12 (m, 6H), 0.72 (t, $J = 7$ Hz, 3H). ^{13}C NMR (100 MHz, CDCl_3): 64.1, 63.9, 48.4, 31.3, 28.8, 28.7, 26.1, 23.8, 22.1, 21.3, 13.7. $T_g = 44.38$ °C. $T_d = 235.17$ °C. HRMS Calcd. for $\text{C}_{13}\text{H}_{28}\text{BrN}$ [M^+]: 278.1479. Found: 278.1483. Anal. Calcd for $\text{C}_{13}\text{H}_{28}\text{BrN}$: C, 56.11; H, 10.14; N, 5.03. Found: C, 56.10; H, 10.14; N, 5.06.

N-methyl-N-(n-octyl)pyrrolidinium bis(trifluoromethanesulfonyl)imide (6). A 40 mL vial was charged with N-methyl-N-octylpyrrolidinium bromide (3.4511 g; 1.24×10^{-2} mol) and water (30 mL). The resulting solution was charged with lithium bis(trifluoromethanesulfonyl)imide (3.5840 g; 1.25×10^{-2} mol) and the vial was sealed with a Teflon-lined cap. After the reaction mixture was stirred for 16 h at room temperature, a clear, pale yellow phase separation formed. The aqueous layer was decanted away and the residual liquid was triturated and sonicated with water (3×30 mL) to remove residual lithium salts dissolved in the product. Subsequent drying under vacuum afforded the desired product as a pale yellow liquid (5.7511 g, 97 % yield). ^1H NMR (400 MHz, CDCl_3): 3.49 (t, $J = 7$ Hz, 4H), 3.26 (t, $J = 7$ Hz, 2H), 2.99 (s, 3H), 2.22 (t, $J = 7$ Hz, 4H), 1.73 (m, 2H), 1.29 (m, 4H), 1.17 (m, 6H), 0.84 (t, $J = 7$ Hz, 3H). ^{13}C NMR (100 MHz, CDCl_3): 119.8 (q, $J = 320$ Hz), 64.7, 64.4, 48.2, 31.5, 28.8, 28.8, 26.0, 23.7, 22.4, 21.4, 13.9. ^{19}F NMR (376 MHz, CDCl_3): -79.0. $T_g = -42.13$ °C. $T_d = 235.47$ °C. HRMS Calcd. for $\text{C}_{13}\text{H}_{28}\text{N}$ [M^+]: 198.2222. Found: 198.2222. Anal. Calcd for $\text{C}_{15}\text{H}_{28}\text{F}_6\text{N}_2\text{O}_4\text{S}_2$: C, 37.65; H, 5.90; N, 5.85. Found: C, 37.90; H, 5.95; N, 5.89.

N-methyl-N-(n-octyl)pyrrolidinium trifluoromethanesulfonate (7). A septum-sealed 40 mL vial was charged with N-methyl-N-(n-octyl)pyrrolidinium bromide (2.2919 g; 8.24×10^{-3} mol) and acetonitrile (20 mL) under nitrogen. The resulting solution was then charged with methyl trifluoromethanesulfonate (1.7404 g; 1.06×10^{-2} mol) slowly via syringe; an exotherm and gas evolution were observed. After stirring the resulting solution for 6 h at room temperature, the solvent was removed under vacuum. The residual solid was triturated and sonicated with diethyl

ether (3×35 mL) to remove unreacted starting materials. Subsequent drying under vacuum afforded the desired product as a tacky, off-white solid (2.6899 g, 94 % yield). ^1H NMR (400 MHz, CDCl_3): 3.51 (t, $J = 7$ Hz, 4H), 3.31 (t, $J = 7$ Hz, 2H), 3.02 (s, 3H), 2.20 (t, $J = 7$ Hz, 4H), 1.74 (m, 2H), 1.24 (m, 4H), 1.09 (m, 6H), 0.82 (t, $J = 7$ Hz, 3H). ^{13}C NMR (100 MHz, CDCl_3): 120.5 (q, $J = 320$ Hz), 64.4, 64.2, 48.1, 31.5, 28.8, 28.4, 26.1, 23.7, 22.4, 21.4, 13.8849. ^{19}F NMR (376 MHz, CDCl_3): -78.6 . $T_g = 17.17$ °C. $T_d = 355.95$ °C. HRMS Calcd. for $\text{C}_{13}\text{H}_{28}\text{N}$ [M^+]: 198.2218. Found: 198.2216. Anal. Calcd for $\text{C}_{14}\text{H}_{28}\text{F}_3\text{NO}_3\text{S}$: C, 48.40; H, 8.12; N, 4.03. Found: C, 48.41; H, 8.07; N, 4.00.

N,N,N-tri-(n-butyl)-N-(n-octyl)ammonium bromide. Using a modified literature procedure,⁴ a 40 mL vial was charged with tri-n-butylamine (4.7597 g; 2.57×10^{-2} mol) and acetonitrile (30 mL; note: tri-n-butylamine is immiscible with acetonitrile). The resulting suspension was charged with 1-bromooctane (5.1740 g; 2.68×10^{-2} mol) and the vial was sealed with a Teflon-lined cap. After the suspension was stirred vigorously at 100 °C for 9 h, the biphasic suspension became homogeneous. The solvent was then removed under reduced pressure and the residual liquid was triturated and sonicated with hexanes (3×30 mL) to remove residual unreacted starting materials. Subsequent drying under vacuum afforded the desired product as a colorless liquid (8.5595 g, 88 % yield). ^1H NMR (400 MHz, CDCl_3): 3.22 (m, 8H), 1.59 (m, 8H), 1.42-1.04 (m, 16H), 0.82 (t, $J = 7$ Hz, 9H), 0.78 (t, $J = 7$ Hz, 3H). ^{13}C NMR (100 MHz, CDCl_3): 59.0, 58.9, 31.4, 28.9, 28.9, 26.2, 24.1, 22.4, 22.1, 19.6, 13.9, 13.6. $T_g = -38.60$ °C. $T_d = 190.16$ °C. HRMS Calcd. for $\text{C}_{20}\text{H}_{43}\text{BrN}$ [M^+]: 376.2584. Found: 376.2579. Anal. Calcd for $\text{C}_{20}\text{H}_{44}\text{BrN}$: C, 63.47; H, 11.72; N, 3.70. Found: C, 63.23; H, 11.74; N, 3.71.

N,N,N-tri-(n-butyl)-N-(n-octyl)ammonium bis(trifluoromethanesulfonyl)imide (8). Using a modified literature procedure,⁵ a 40 mL vial was charged with N,N,N-tributyl-N-octylammonium bromide (5.3567 g; 1.42×10^{-2} mol) and water (30 mL). The resulting solution was then charged with lithium bis(trifluoromethanesulfonyl)imide (4.1892 g; 1.46×10^{-2} mol) and the vial was sealed with a Teflon-lined cap. After the reaction mixture was stirred at room temperature for 16 h, a clear, pale, yellow phase separation formed. The aqueous layer was decanted away and the residual liquid was triturated and sonicated with water (3×30 mL) to remove residual lithium salts dissolved in the product. Subsequent drying under vacuum afforded the desired product as a pale yellow liquid (7.8878 g, 96 % yield). ^1H NMR (400 MHz,

CDCl₃): 3.15 (m, 8H), 1.60 (m, 8H), 1.18-1.41 (m, 16H), 0.95 (t, $J = 7$ Hz, 9H), 0.82 (t, $J = 7$ Hz, 3H). ¹³C NMR (100 MHz, CDCl₃): 119.9 (q, $J = 320$ Hz), 59.1, 58.5, 31.5, 28.9, 28.9, 26.0, 23.7, 22.5, 21.7, 19.4, 14.0, 13.4. ¹⁹F NMR (376 MHz, CDCl₃): -78.9. $T_g = -63.23$ °C. $T_d = 376.85$ °C. HRMS Calcd. for C₂₀H₄₄N [M⁺]: 298.3477. Found: 298.3474. Anal. Calcd for C₂₂H₄₄F₆N₂O₄S₂: C, 45.66; H, 7.66; N, 4.84. Found: C, 45.87; H, 7.72; N, 4.97.

N,N,N-tri-(n-butyl)-N-(n-octyl)ammonium trifluoromethanesulfonate (9). Using a modified literature procedure,^{5b} a 40 mL septum-sealed vial was charged with N,N,N-tri-(n-butyl)-N-(n-octyl)ammonium bromide (2.5421 g; 6.72×10^{-3} mol) and dichloromethane (35 mL) under nitrogen. The resulting solution was charged with methyl trifluoromethanesulfonate (1.3746 g; 8.38×10^{-3} mol) slowly via syringe; an exotherm and gas evolution were observed. After the reaction mixture was stirred at room temperature for 6 h, the solvent was removed under reduced pressure. The residual solid was triturated and sonicated with diethyl ether (3×35 mL) to removed unreacted starting materials. Subsequent drying under vacuum afforded the desired product as an off-white viscous liquid (2.9466 g, 98 % yield). ¹H NMR (400 MHz, CDCl₃): 3.17 (m, 8H), 1.56 (m, 8H), 1.38 (p, 6H), 1.25 (m, 10H), 0.97 (t, $J = 7$ Hz, 9H), 0.85 (t, $J = 7$ Hz, 3H). ¹³C NMR (100 MHz, CDCl₃): 120.5 (q, $J = 320$ Hz), 58., 58.4, 31.5, 28.8, 28.8, 26.1, 23.7, 22.4, 21.7, 19.4, 13.9, 13.4. ¹⁹F NMR (376 MHz, CDCl₃): -78.8. $T_g = -56.82$ °C. $T_d = 322.45$ °C. HRMS Calcd. for C₂₀H₄₄N [M⁺]: 298.3477. Found: 298.3467. Anal. Calcd for C₂₁H₄₄F₃NO₃S: C, 56.35; H, 9.91; N, 3.13. Found: C, 56.48; H, 9.89; N, 3.04.

Characterization of Mesoporous Carbon Capsules. The carbon capsules (prepared as previously reported⁶) were characterized by SEM (Figure S1), PXRD (Figure S3; PXRD was carried out at room temperature at a relative humidity of approximately 45%) and N₂ adsorption isotherms (Figure S4). The powder conductivity was measured to be 330 S·m⁻¹ using a previously described procedure.⁷ TEM images of the mesoporous carbon nanocapsules employed can be seen in ref. 6.

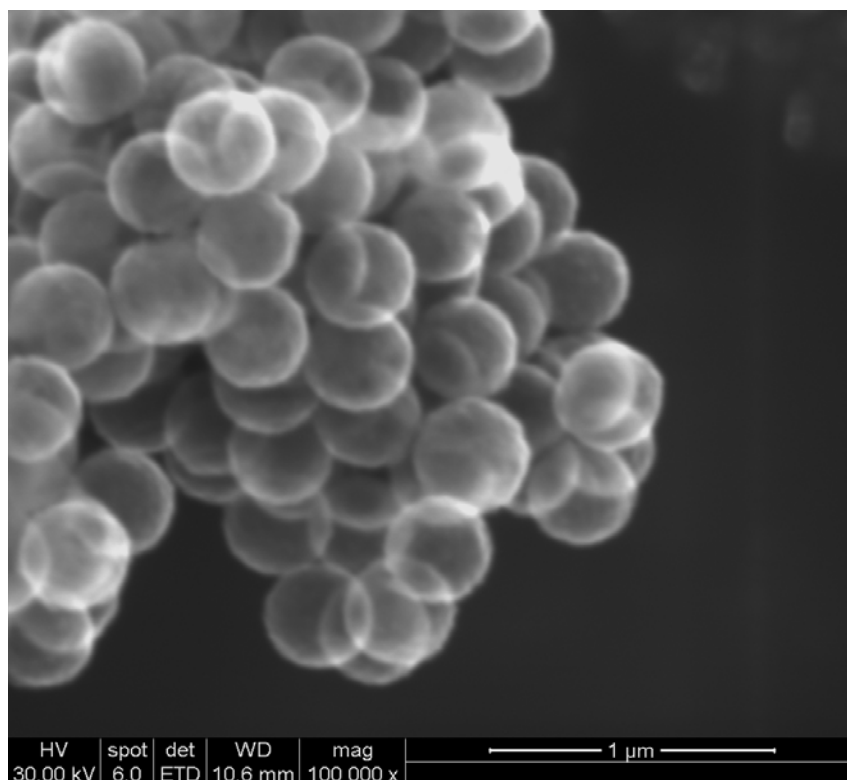


Figure S1. Scanning electron microscopy (SEM) image of mesoporous carbon nanocapsules.

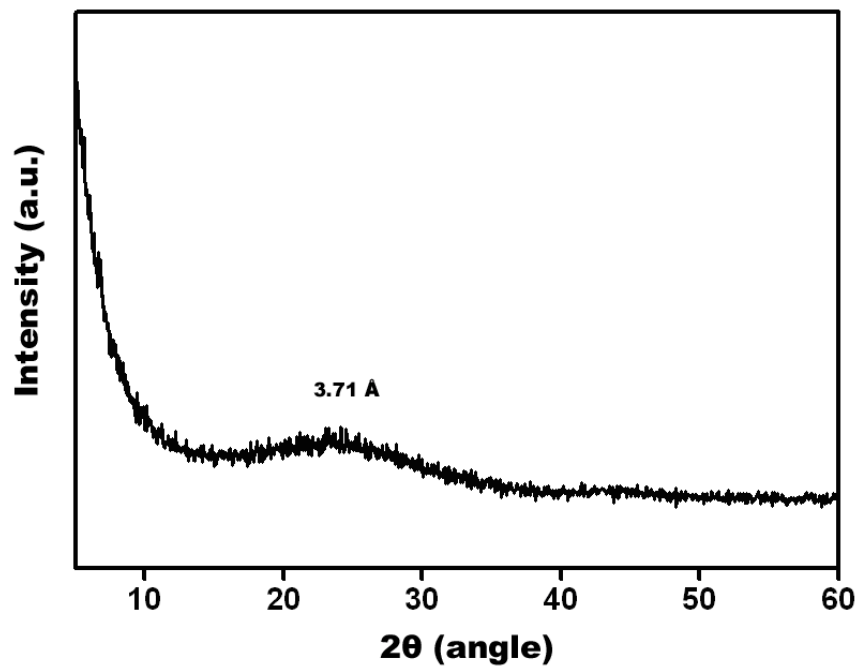


Figure S2. Powder X-ray diffraction (PXRD) plot of mesoporous carbon nanocapsules showing a broad peak centered at $2\theta = 24^\circ$ (d-spacing = 3.71 Å).

Electrochemical Double Layer Capacitor (EDLC) Testing. A two-electrode cell configuration was used to measure the performance of the EDLC using the carbon capsules (Figures S6–S14), as well as microwave exfoliated graphite oxide (MEGO; Figure S15) and chemically-reduced graphene oxide (CReGO; Figure S16) as electrodes. MEGO and CReGO were prepared using methods previously reported.^{7,8} Polytetrafluoroethylene (PTFE; 5 wt% dispersion in water) was added to the powder as a binder. The mixture of carbon capsules and PTFE was ground, rolled into 75 μm thick sheets and punched into 1 cm diameter electrodes. The electrodes were tested in a two electrode test cell assembly (Figure S3), which consisted of two current collectors, two electrodes, and an ion-porous separator (Celgard[®] 3501) supported in a test fixture consisting of two stainless steel plates. A conductive vinyl collector material (Exopack[™] 2.35 mil vinyl [Product #2267]) was used with the aqueous electrolyte and a conductive carbon coated aluminum foil (Exopack[™] 0.5 mil 2-side coating) was used with organic and IL electrolytes.

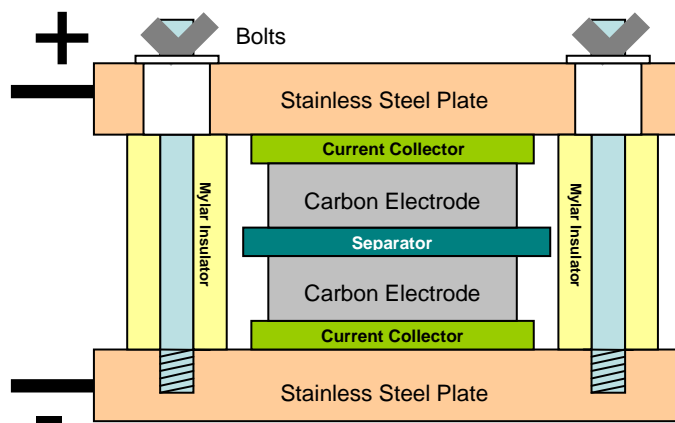


Figure S3. Schematic of two-electrode test cell assembly.

The aqueous electrolyte (KOH) was prepared at a 6 M concentration in water. The tetraethylammonium tetrafluoroborate (TEA BF₄) was prepared at 1 M in acetonitrile (AN) and the 1-butyl-3-methylimidazolium hexafluorophosphate (BMIM PF₆) was obtained commercially from Sigma Aldrich. All other ILs were prepared as described previously (see main text). AN (20 vol%) was added to the ionic liquids with melting points or glass transition temperatures

greater than room temperature to decrease the melting point and viscosity of the IL, and also to increase the wettability of electrodes.

Capacitance values were calculated from the CV curves by dividing the measured current by the applied scan rate, according to Eq. 1.

$$C = \frac{I}{dV/dt} \quad \text{Eq. 1}$$

Capacitance from galvanostatic charge/discharge was calculated by dividing the applied constant current by the measured change in potential (Eq.1), with dV/dt calculated from the slope obtained by fitting a straight line to the discharge curve. Specific capacitance was calculated by normalizing the measured capacitance with the mass of carbon capsules in one electrode.

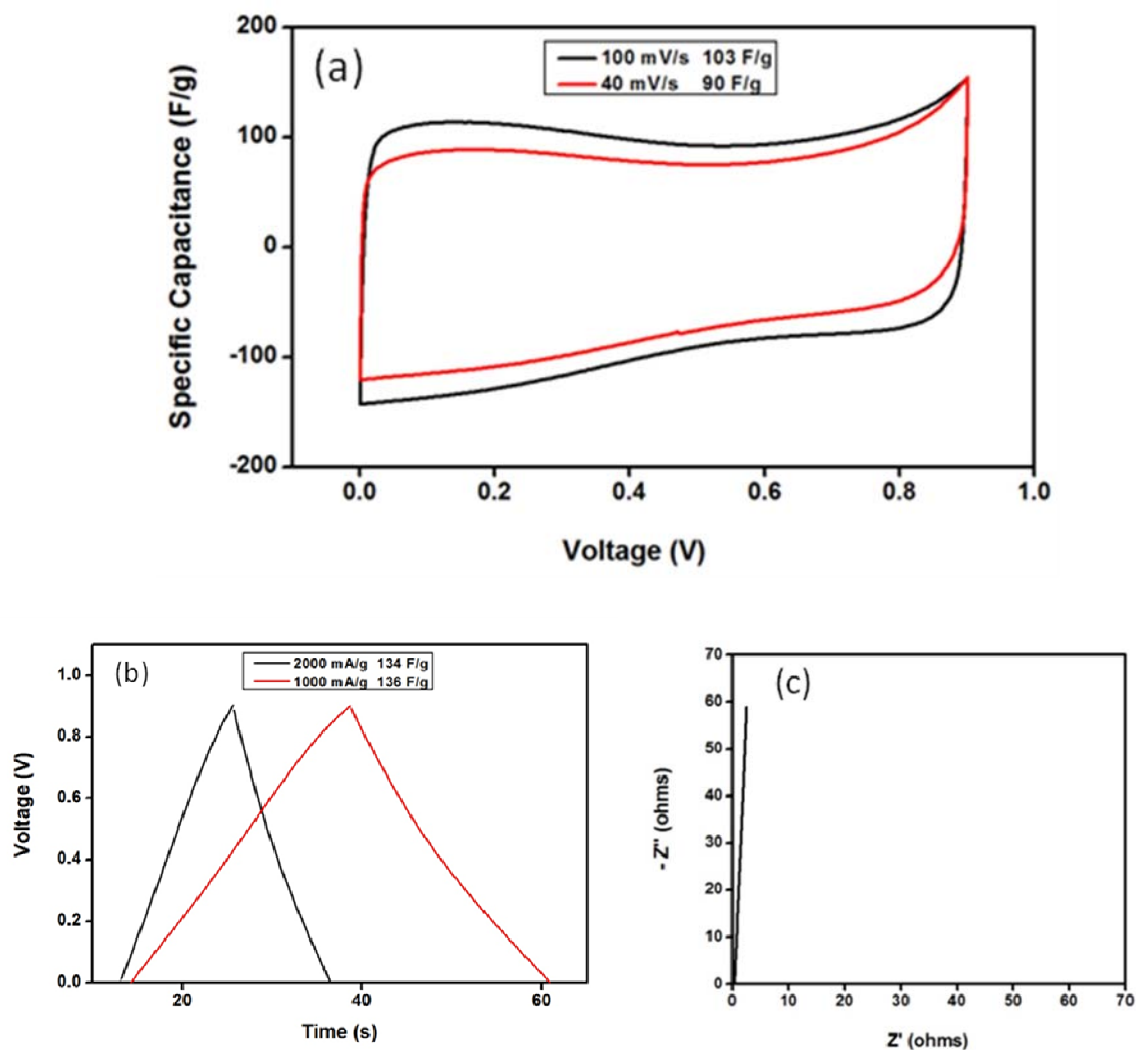


Figure S4. EDLC performance of the carbon capsules in aq. KOH (6 M); (a) cyclic voltammograms at scan rates of 40 and 100 $\text{mV}\cdot\text{s}^{-1}$; (b) galvanostatic charge-discharge curve at current densities of 1000 and 2000 $\text{mA}\cdot\text{g}^{-1}$ and (c) Nyquist plot ($0.02 \text{ Hz} < \nu < 1 \text{ MHz}$) used to characterize the internal cell resistance.

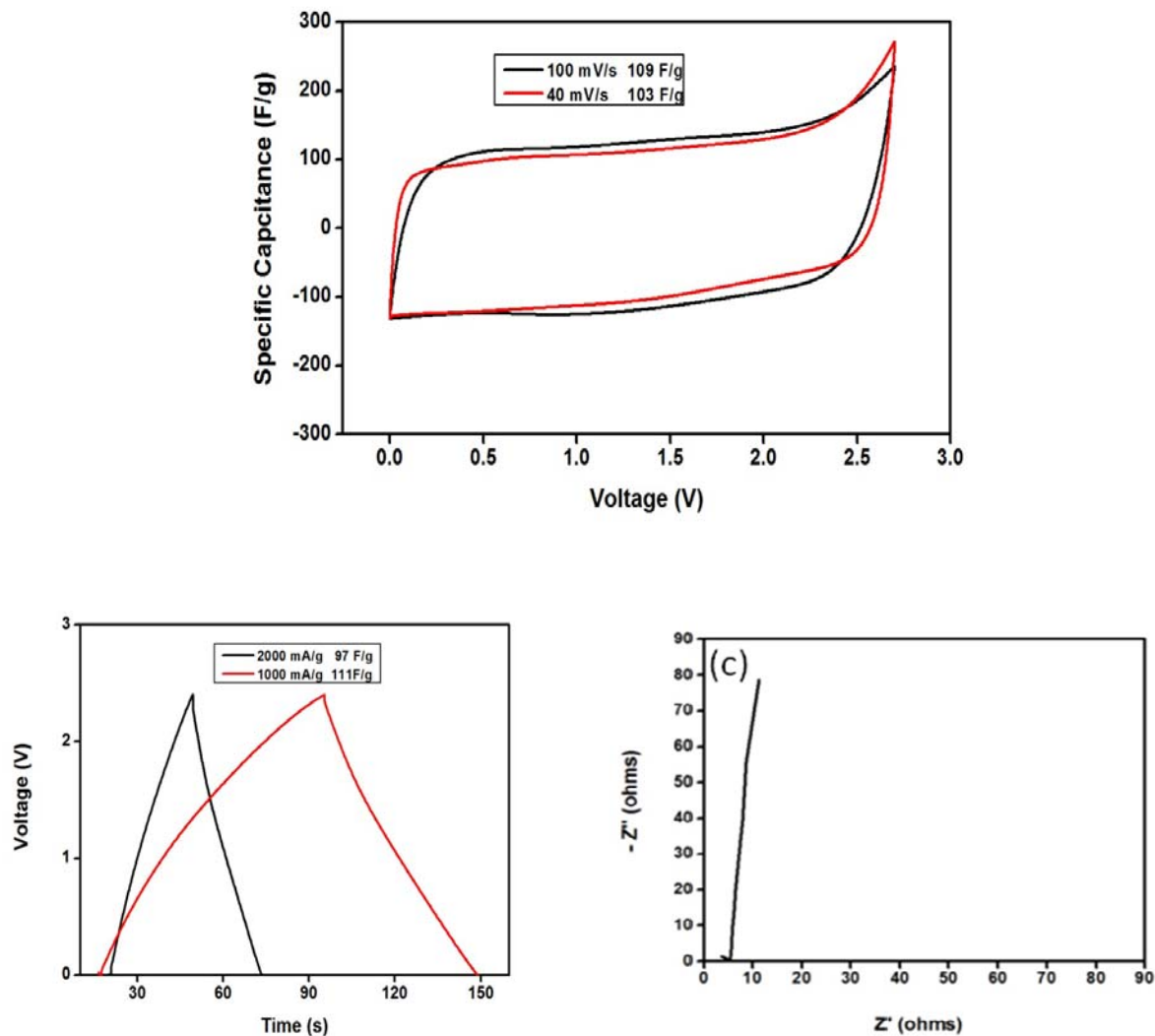


Figure S5. EDLC performance of the carbon capsules in TEA BF₄ in AN (1 M); (a) cyclic voltammetry curves at scan rates of 40 and 100 mV·s⁻¹; (b) galvanostatic charge-discharge curve at current densities of 1000 and 2000 mA·g⁻¹ and (c) Nyquist plot (0.02 Hz < ν < 1 MHz) used to characterize the internal cell resistance.

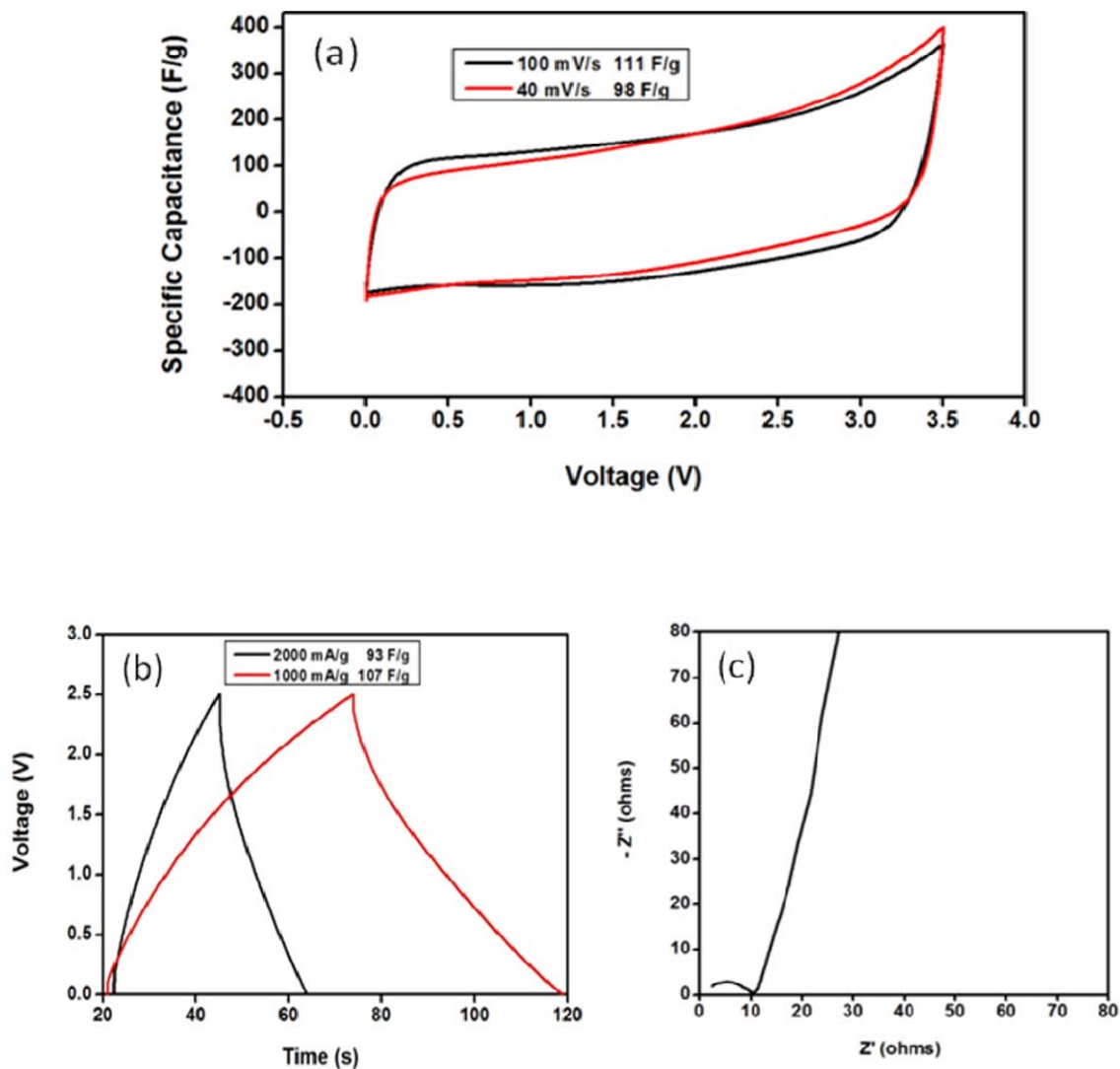


Figure S6. EDLC performance of the carbon capsules in IL 3 (BMIM PF₆); (a) cyclic voltammetry curves at scan rates of 40 and 100 mV·s⁻¹; (b) galvanostatic charge-discharge curve at current densities of 1000 and 2000 mA·g⁻¹ and (c) Nyquist plot (0.02 Hz < ν < 1 MHz) used to characterize the internal cell resistance.

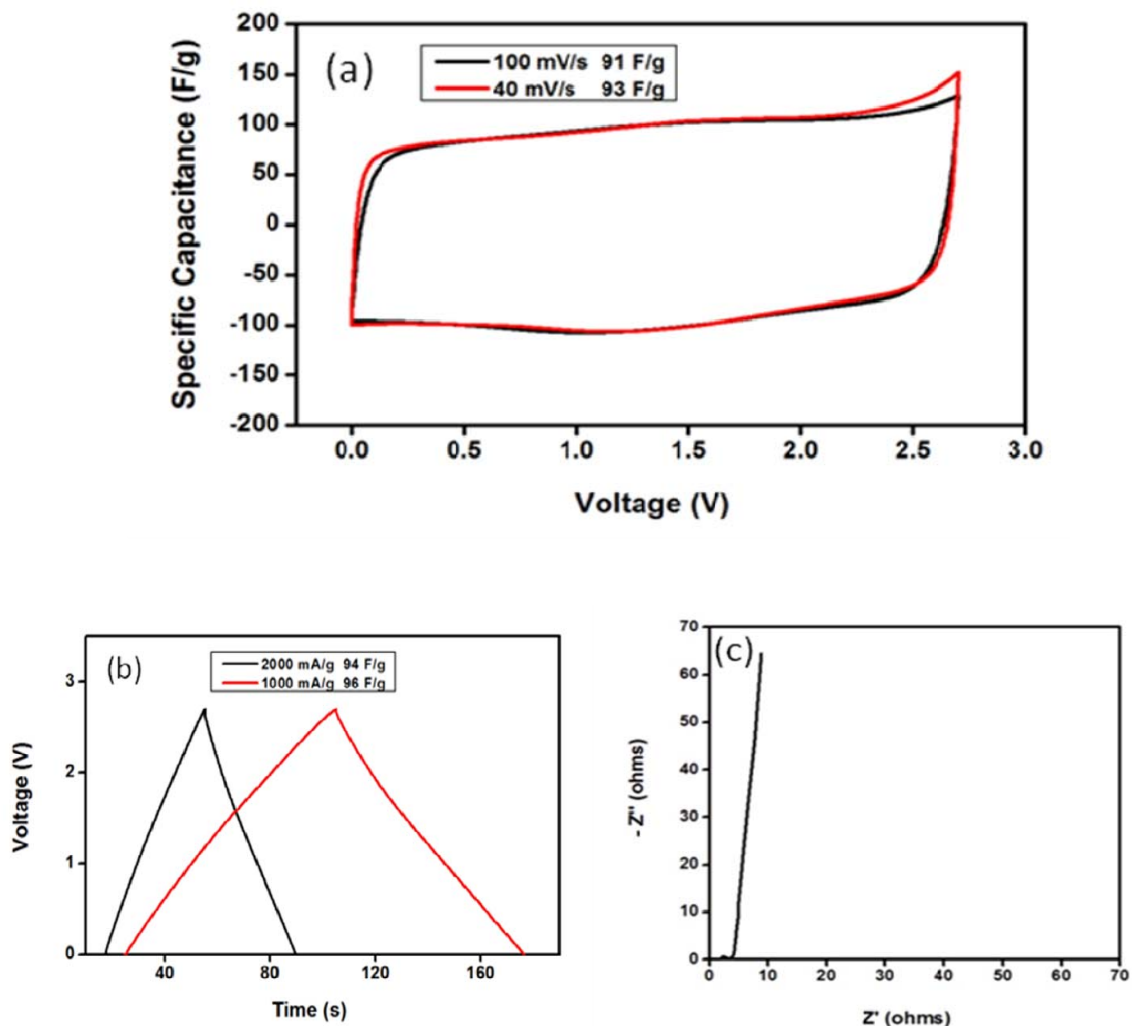


Figure S7. EDLC performance of the carbon capsules in IL 4; (a) cyclic voltammetry curves at scan rates of 40 and 100 $\text{mV}\cdot\text{s}^{-1}$; (b) galvanostatic charge-discharge curve at current densities of 1000 and 2000 $\text{mA}\cdot\text{g}^{-1}$ and (c) Nyquist plot ($0.02 \text{ Hz} < \nu < 1 \text{ MHz}$) used to characterize the internal cell resistance.

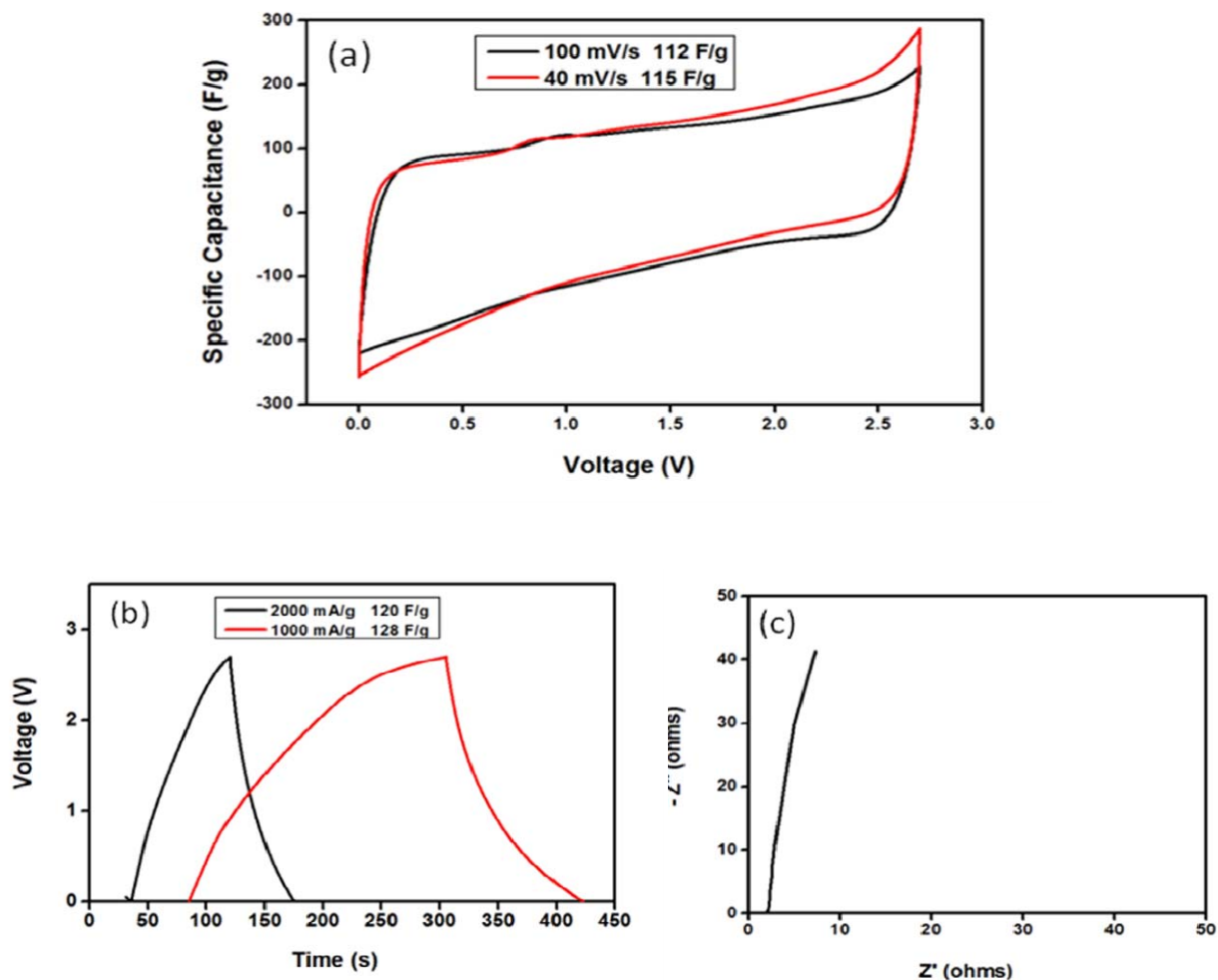


Figure S8. EDLC performance of the carbon capsules in IL 5 (diluted with 20 wt% AN); (a) cyclic voltammograms at scan rates of 40 and 100 $\text{mV}\cdot\text{s}^{-1}$; (b) galvanostatic charge-discharge curve at current densities of 1000 and 2000 $\text{mA}\cdot\text{g}^{-1}$ and (c) Nyquist plot ($0.02 \text{ Hz} < \nu < 1 \text{ MHz}$) used to characterize the internal cell resistance.

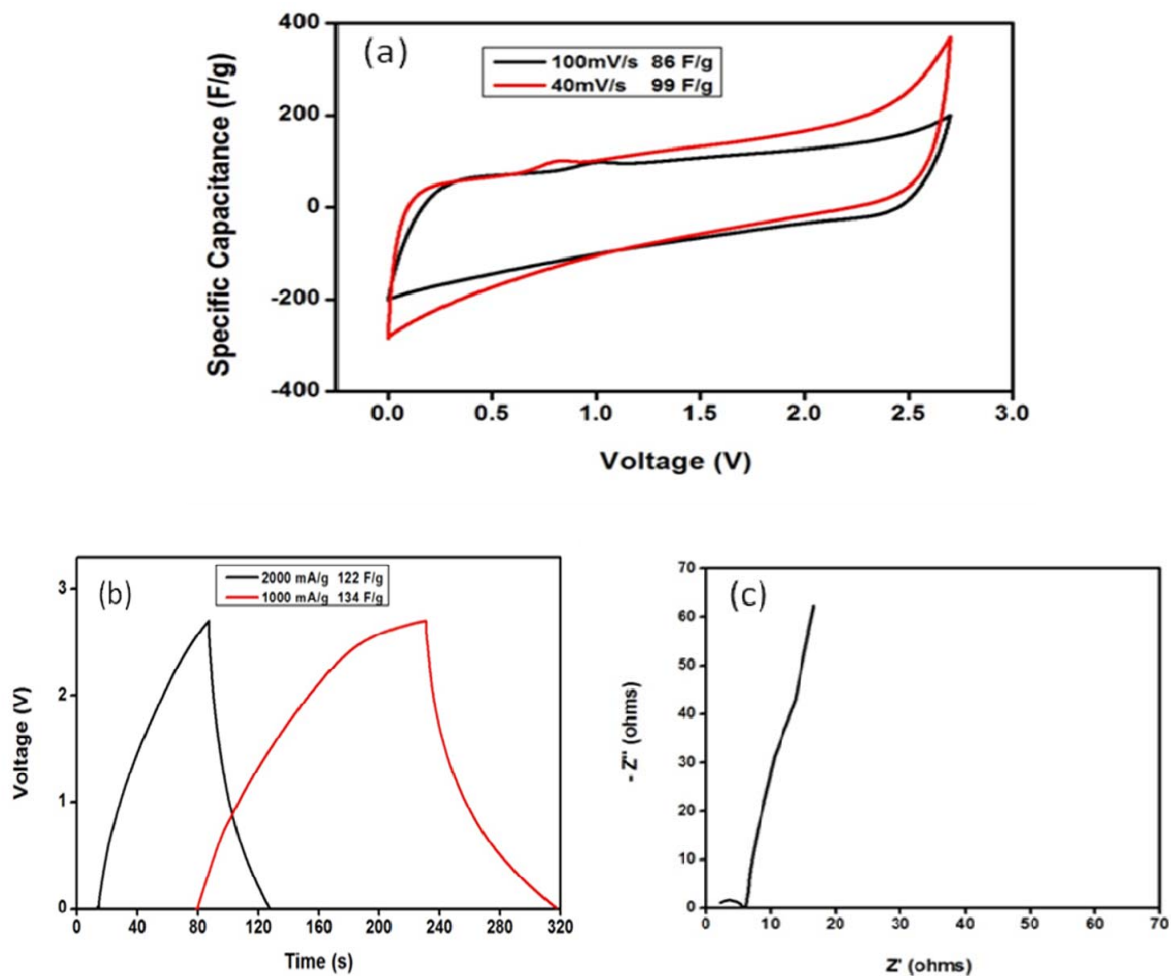


Figure S9. EDLC performance of the carbon capsules in IL 7 (diluted with 20 wt% AN); (a) cyclic voltammetry curves at scan rates of 40 and 100 $\text{mV}\cdot\text{s}^{-1}$; (b) galvanostatic charge-discharge curve at current densities of 1000 and 2000 $\text{mA}\cdot\text{g}^{-1}$ and (c) Nyquist plot ($0.02 \text{ Hz} < \nu < 1 \text{ MHz}$) used to characterize the internal cell resistance.

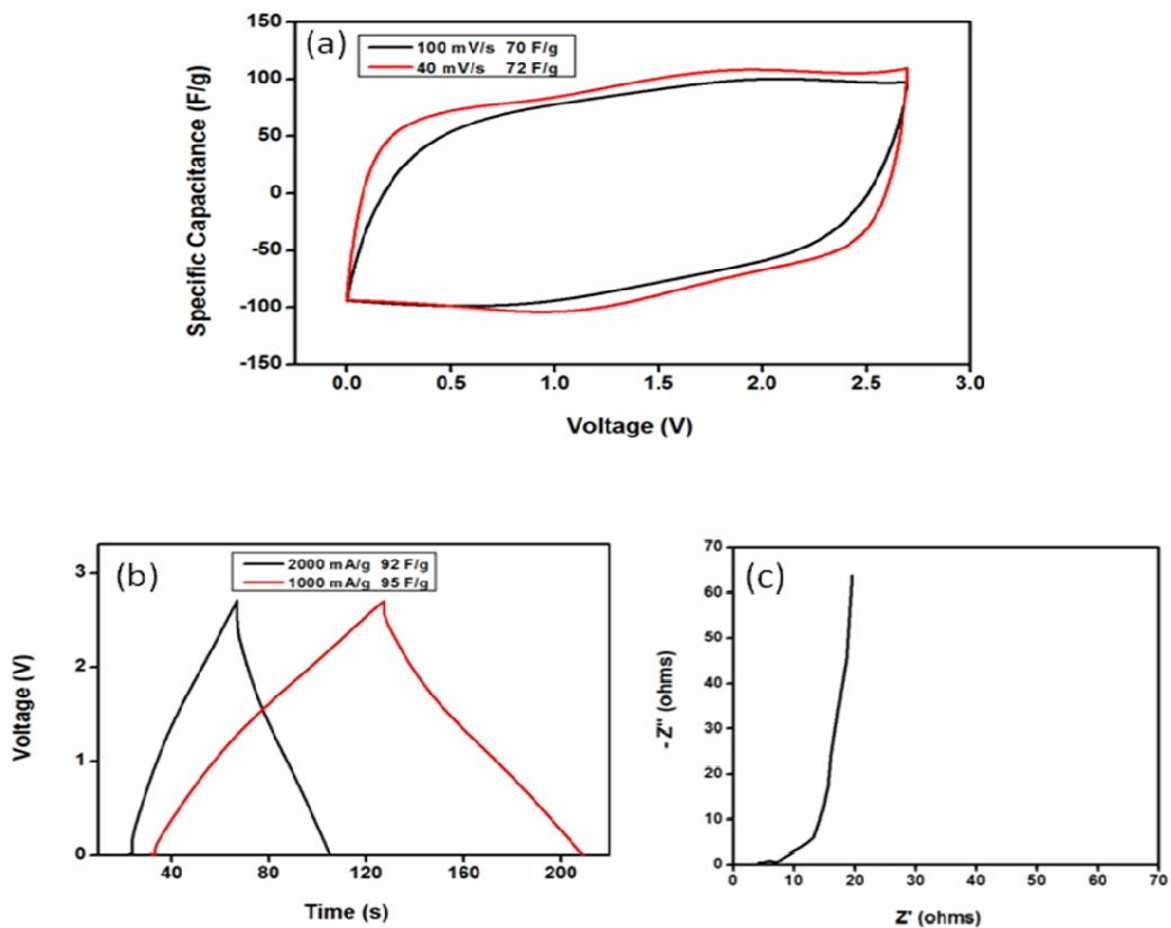


Figure S10. EDLC performance of the carbon capsules in IL 8; (a) cyclic voltammetry curves at scan rates of 40 and 100 $\text{mV}\cdot\text{s}^{-1}$; (b) galvanostatic charge-discharge curve at current densities of 1000 and 2000 $\text{mA}\cdot\text{g}^{-1}$ and (c) Nyquist plot ($0.02 \text{ Hz} < \nu < 1 \text{ MHz}$) used to characterize the internal cell resistance.

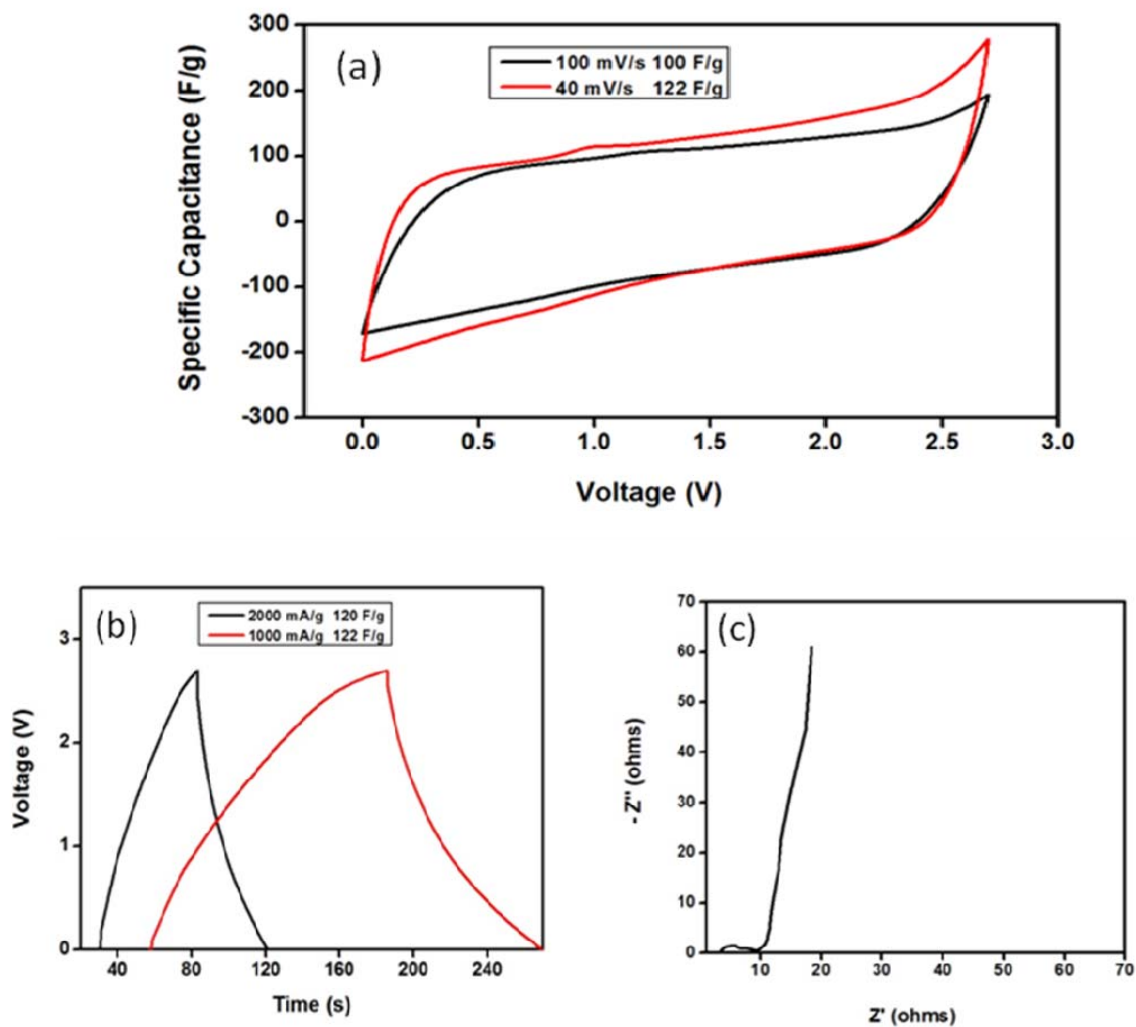


Figure S11. EDLC performance of the carbon capsules in IL **9**; (a) cyclic voltammetry curves at scan rates of 40 and 100 $\text{mV}\cdot\text{s}^{-1}$; (b) galvanostatic charge-discharge curve at current densities of 1000 and 2000 $\text{mA}\cdot\text{g}^{-1}$ and (c) Nyquist plot ($0.02 \text{ Hz} < \nu < 1 \text{ MHz}$) used to characterize the internal cell resistance.

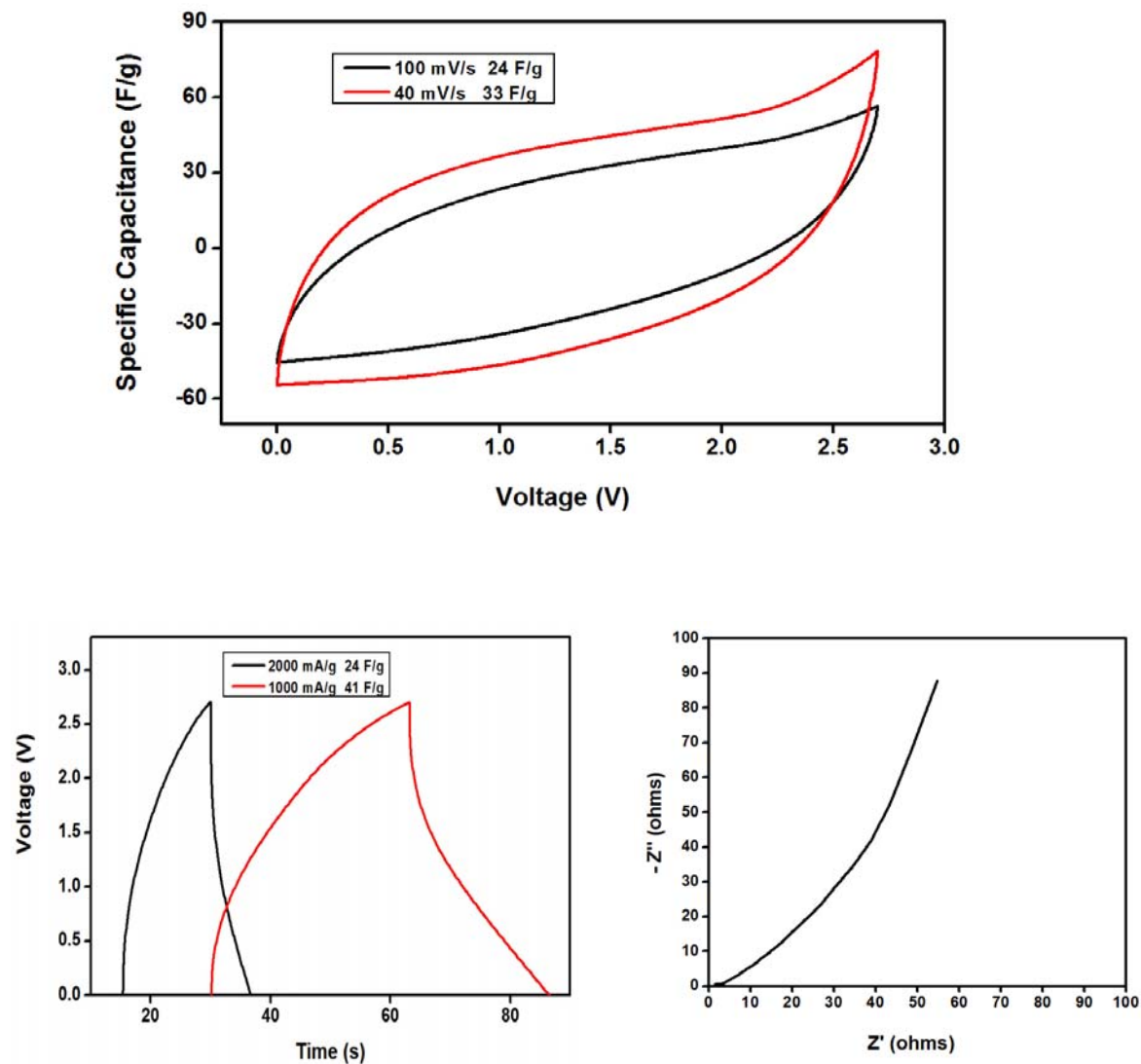


Figure S12. EDLC performance of the MEGO in IL 6; (a) cyclic voltammetry curves at scan rates of 40 and 100 $\text{mV}\cdot\text{s}^{-1}$; (b) galvanostatic charge-discharge curve at current densities of 1000 and 2000 $\text{mA}\cdot\text{g}^{-1}$ and (c) Nyquist plot ($0.02 \text{ Hz} < \nu < 1 \text{ MHz}$) used to characterize the internal cell resistance.

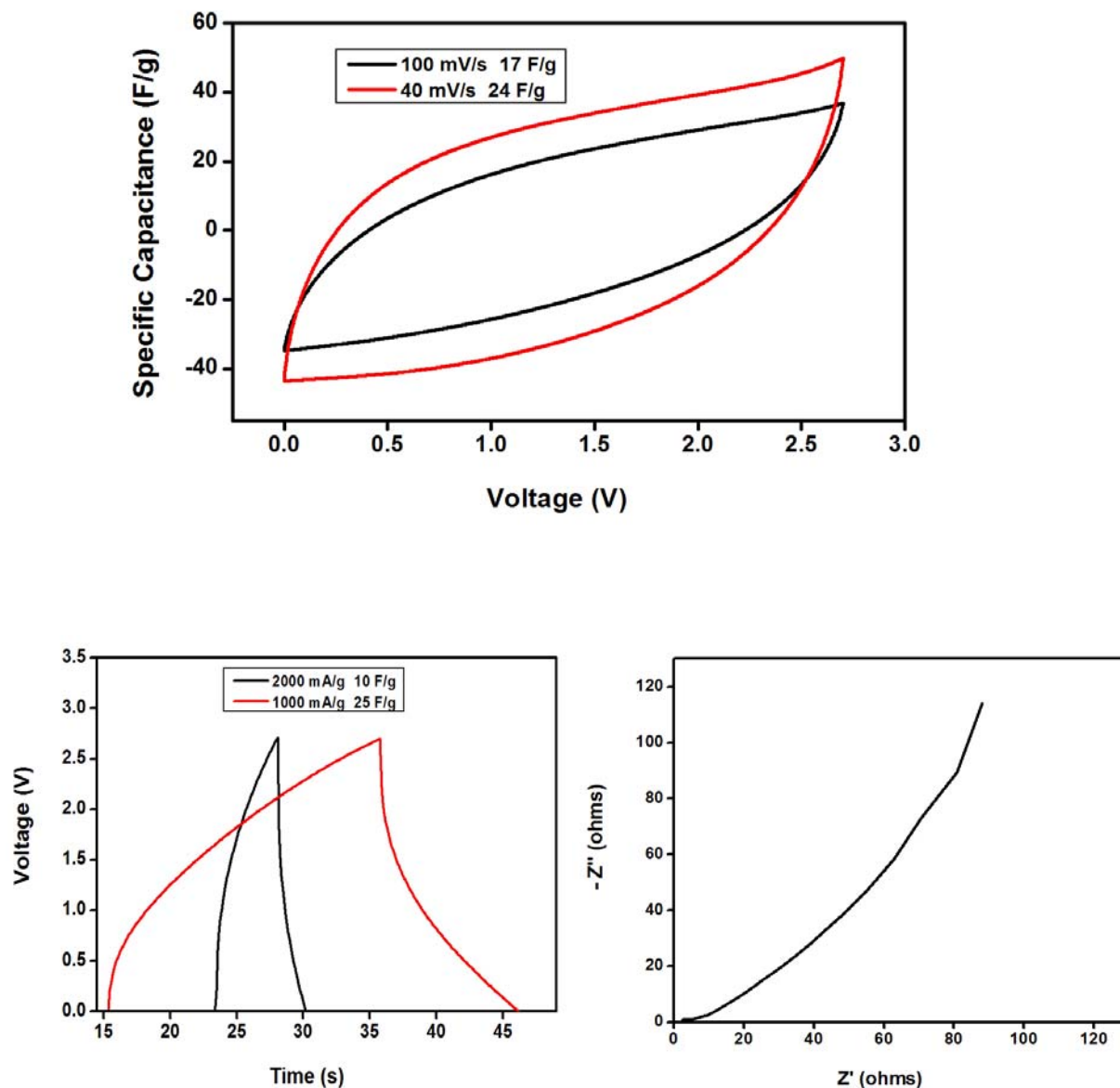


Figure S13. EDLC performance of the CReGO in IL 6; (a) cyclic voltammetry curves at scan rates of 40 and 100 $\text{mV}\cdot\text{s}^{-1}$; (b) galvanostatic charge-discharge curve at current densities of 1000 and 2000 $\text{mA}\cdot\text{g}^{-1}$ and (c) Nyquist plot ($0.02 \text{ Hz} < \nu < 1 \text{ MHz}$) used to characterize the internal cell resistance.

References

1. A. Triolo, O. Russina, B. Fazio, G. B. Appetecchi, M. Carewska and S. Passerini, *J. Chem. Phys.*, 2009, **130**, 164521.
2. J. Salminen, N. Papaiconomou, R. A. Kumar, J.-M. Lee, J. Kerr, J. Newman and J. M. Prausnitz, *Fluid Phase Equilib.*, 2007, **261**, 421–426.
3. K. Goossens, K. Lava, P. Nockemann, K. Van Hecke, L. Van Meervelt, K. Driesen, C. Görrler-Walrand, K. Binnemans and T. Cardinaels, *Chem. Eur. J.*, 2009, **15**, 656–674.
4. J. Yao, S. Lei, J. Huang, Y. Feng and Z. Li, *Langmuir*, 2006, **22**, 9526–9531.
5. (a) J. Sun, M. Forsyth and D. R. MacFarlane, *J. Phys. Chem. B*, 1998, **102**, 8858–8864 . (b) J. Sun, D. R. MacFarlane and M. Forsyth, *Ionics*, 1997, **3**, 356–362.
6. P. Valle-Vigón, M. Sevilla and A. B. Fuertes, *Chem. Mater.*, 2010, **22**, 2526–2533.
7. Y. Zhu, S. Murali, M. D. Stoller, A. Velamakanni, R. D. Piner and R. S. Ruoff, *Carbon*, 2010, **48**, 2118–2122.
8. S. Stankovich, D. A. Dikin, R. D. Piner, K. A. Kohlhaas, A. Kleinhammes, Y. Jia, Y. Wu, S. T. Nguyen and R. S. Ruoff, *Carbon*, 2007, **45**, 1558.